New keratose sponges after the end-Permian extinction provide insights into biotic recoveries

Abstract

We challenge the prevailing view that the end-Permian extinction impeded the Triassic evolution of sponges. Here we report a deep-water community dominated by abundant keratose sponges in the lowest Triassic strata from Southwest China. The sponge fossils occur as dark elliptical imprints in mudstone with distinct oscula on their tops. The structure of preserved fibers suggests closest affinity with the extant Dictyoceratida, an aspiculate demosponge. The exceptional preservation plays a crucial role in retaining their exquisite structures. Sedimentary, taphonomic, pyrite framboid, and trace elemental analyses indicate that the sponges proliferated in an oxygen-poor habitat, demonstrating the high tolerance of sponges to severe conditions. Sponge proliferation is a signal of environmental upheaval but they also stabilized the ecosystem, driving the first phase of biotic recovery after the end-Permian extinction.

Key words: keratose sponge, environmental stress, recovery, end-Permian extinction, Southwest China

1 INTRODUCTION

The end-Permian extinction severely depleted marine biodiversity, and both

oxygen-poor and poisonous conditions prevailed in the earliest Triassic oceans, delaying biotic recovery (Chen and Benton, 2012; Huang et al., 2023); oceanographic conditions after the end-Permian crisis were far from ideal for the colonization of the seabed. Sponges, particularly those reef-building groups, suffered dramatic losses during the crisis (Finks, 2010). Global range charts show that sponges overall experienced an evolutionary gap in the aftermath of the end-Permian crisis (Velledits, 2008; Finks, 2010), although there are sporadic reports of this clade from the Lower Triassic in western US and southern China (Brayard et al., 2017; Dai et al., 2023). Previous studies have reported some keratose sponge-like textures occasionally occurring in microbialites near the Permian−Triassic (P−Tr) boundary (Friesenbichler et al., 2018; Heindel et al. 2018; Baud et al., 2021; Wu et al., 2022). Similar keratose sponge-like fibers have received significant attention in recent years (e.g., Luo and Reitner, 2014; Luo et al., 2022; Lee and Riding, 2021; 2023) and have been found in an 890-million-year-old carbonate build up (Turner, 2021). However, such interpretations remain questionable (Neuweiler et al., 2023), and the identification of aspiculate sponge in other facies is much more challenging. Thus, previous records of keratose sponge fossils require critical appraisal to substantiate their reliability, and the survival status of sponges in earliest Triassic still remains obscure.

Here, we report abundant, well-preserved aspiculate sponges, together with abundant brachiopods and ammonoids from the lowest Triassic (Griesbachian) in the Kejiao section, Guizhou Province, South China. These fossils unexpectedly occurred immediately after the end-Permian extinction with a mode of preservation that agrees

well with Lagerstätte forms. Moreover, the taphonomic window of the Kejiao section, links low oxygen conditions with exceptional preservation similar to that of many Cambrian Lagerstätten (Harper et al., 2019; Zheng et al., 2022), and is compatible with the hypoxia tolerance of sponges.

2 GEOLOGICAL SETTING

The new sponge fossils were collected from the lowest Triassic strata in the Kejiao section of Huishui County, Guizhou Province, southwest China (Figure S1a), located in the northern Nanpanjiang Basin of the southern South China block that was situated at low latitudes in the eastern Paleo-Tethys region during the earliest Triassic (Enos et al., 2006; He et al., 2022; Figure 1). The upper Permian Talung Formation is composed of siliceous mudstone and carbonaceous shales, interbedded with tuff and calcareous mudstone (Figure 2), whereas the Lower Triassic Luolou Formation is dominated by yellowish mudstone and calcareous mudstone, with several layers of grayish green marlstone at the base. The Talung Formation yields abundant cephalopods, bivalves, brachiopods, radiolarians, foraminiferans, and sponge spicules. The cephalopod fauna including *Pseudotirolites* and *Pleuronodoceras*, indicates a latest Changhsingian age (Jiang et al., 2018). Fossil assemblages, along with the presence of laminations and distal Bouma turbidite sequences, indicate a deep-water environment (Wang et al., 2023). The Luolou Formation bed 74 to bed 83 is characterized by the presence of the ammonoids *Ophiceras* spp. and bivalve *Claraia*

wangi, assignable to the *Claraia wangi-C. gresbachi* assemblage and *Ophiceras* assemblage, respectively, equivalent to the conodont *Isarcicella staeschei* Zone to the *I. isarcica* Zone in the Meishan section, South China (Chen et al., 2015), which is the Global Stratotype Section and Point (GSSP) for the P−Tr boundary (PTB) (Yin et al., 2001; Shen et al., 2022), indicating an early Griesbachian age. The PTB therefore is placed at the base of Bed 74 in the Kejiao section (Wang et al., 2023).

The new sponge fossils, in association with an undentifiable species of the ammonoid *Ophiceras*, bivalve *Claraia wangi* and brachiopod *Meishanorhynchia* (Chen et al., 2002; Guo et al., 2022), occur in strata 4.5−6 m above the PTB, beds 82-84 in Luolou Formation (Figure 2, blue bar), and are therefore early Griesbachian in age.

MATERIAL AND METHODS

A total of 100 slabs were collected from 10 layers within the 1.5-m-thick sponge-bearing strata in Kejiao, and >600 well-preserved sponge individuals were measured. Taxonomic identification follows Antcliffe et al. (2014), with comparison with morphological features of modern sponge specimens illustrated in 'The Sponge Guide' (Zea et al., 2014) and dried specimens of modern sponges from the authors' personal collections.

Microfacies analysis and the paleoenvironmental interpretation were prepared based on observations of conventional petrologic thin-sections. To assess redox

conditions, 22 Kejiao samples were prepared for whole-rock trace element analysis (Figure 2). The trace element analysis was performed at Wuhan Sample Solution Analytical Technology Co., Ltd. using Agilent 7700e ICP-MS. V/Cr and V/ (V + Ni) ratios are ideal indices of redox conditions in ancient mudstones (Hatch and Leventhal, 1992; Jones and Manning, 1994). The V/Cr ratio varied through oxic (< 2), dysoxic (2~4.25) and anoxic (> 4.25) conditions (Jones and Manning, 1994). The V/(V+Ni) ratio varied through dysoxic (0.46~0.60), anoxic (0.54~0.82) and euxinic (> 0.84) conditions (Hatch and Leventhal, 1992).

A total of 60 rock samples from 22 horizons were collected for pyrite framboid analysis to help unravel the P−Tr redox history of the Kejiao succession. Pyrite framboids were observed and measured by scanning electron microscopy (SEM, Hitachi SU8000) at the State Key Laboratory of Biogeology and Environmental Geology (BGEG) in the China University of Geosciences (Wuhan). Criteria for the relationships between framboid size distributions and morphology, and redox states follow Bond and Wignall (2010). Dispersed framboids instead of clustered framboids are chosen to minimize the influence of diagenesis (Huang et al., 2017, 2019).

Well-preserved sponge samples were selected for Raman analysis using the WiTec alpha300 R confocal Raman spectrometer at the University of Göttingen in Germany. The Raman spectra were obtained under a 532 nm wavelength laser at a power of 4.974 mW in a range of 75–4000 cm^{-1} at a 1 cm^{-1} resolution (Jing et al., 2022).

4 RESULTS

4.1 Description of sponge fossils

Abundant sponge individuals are densely packed on the slab surfaces, showing a lack of preferred size or orientation (Figure 3a; Figure S2). Fragmentation ratio is low, only in 8.5% of 600 individuals. The new sponge fossils have a high abundance, blanketing the entire mudstone layer, sometimes covering up to >75 % of the surface (Figure 3a) and are dominated by one new taxon together with minor elements, including one brachiopod species and ammonoids. Sponge specimens are flattened, presented as circular-to-elliptical, thin carbonaceous films on mudstone surfaces, but preserving three-dimensional features (Figure 3f). A fragmented fossil specimen displays the thickness of the lateral wall, with the mesh penetrating through the lateral walls (Figure 3f). The fossils are composed of reticulate, organic networks (spongin skeleton), lacking identifiable spicules. The residual sponge material, overall, is sack-shaped with a circular opening on the top serving as an osculum (Figure 3; red arrows), which is typical of sponges. Complete individuals are 2−16 mm (average 5.6 mm) wide and 3−30 mm (average 8.7 mm) high, with height/width ratios of 0.9−3. Oscula are 1−5 mm in diameters, occupying 20−70 % of sponge width. Organic frameworks are 0.5−1 mm wide.

The budding process of Kejiao sponges was preserved, manifest as an outgrowth from the parent body (Figure 3k-m). At the junction of the bud and the mother sponge, the base of the bud is slightly narrowed, while the bases of other ordinary individuals

are round and smooth, indicating that the narrow base is characteristic of the connection between the bud and the mother, rather than the two individuals simply overlapping. Therefore, this phenomenon may be due to the fact that the budding reproductive process of sponges has just been preserved. Budding is a common mode of asexual reproduction in sponges, representing an important reproductive strategy for some species, and maximizing the dispersal of these animals (Gaino et al., 2006). The Kejiao fossils represent the first record of budding reproduction in ancient keratose sponges.

The preserved fibers show thick primary and thinner secondary structures, suggesting that they represent a new keratose aspiculate demosponge which exhibits a best fit with the extant Dictyoceratida (see details in Supplementary materials, Figure 4). A new genus and new species *Palaeosmenospongia kejiaoensis* n. gen, n. sp. is proposed. However, though the spongin network is well preserved, other soft tissues (e.g. epidermal cells) are not, which limit any valid data about the soft tissue function.

Raman spectroscopy is employed to understand the taphonomic pathway of the sponge material. The Raman spectra of the dark fossil remains possess two distinct bands at wave-length numbers 1350 cm^{-1} and 1580 cm^{-1} (Figure 5c-f), typical of organic carbon (Ferrari and Robertson, 2000; Jing et al., 2022). D (disordered carbon) and G (graphite) bands are very sharp and indicate strong maturation of the organic carbon, while the Raman spectra of the surrounding mudstone lack such bands. No silica signal was observed.

4.2 Systematic paleontology

Phylum Porifera Grant, 1836

Class Demospongiae Sollas, 1875

Order Dictyoceratida Minchin, 1900

Family Thorectidae Bergquist, 1978

Genus *Palaeosmenospongia* n. gen. Wu & Reitner

Type species. *Palaeosmenospongia kejiaoensis* n. gen., n. sp. Wu & Reitner

Etymology. Combined from "*palaeo*" = old (Latin) and "*Smenospongia*", a comparable extant genus of the Family Thorectidae.

Diagnosis. Vase to cup shaped centimeter-sized sponges, with a large central osculum and a network of thick and thin fibers commonly crowded and interconnected; it is possible to distinguish between thick primary and thinner secondary fibers. The organic skeleton is thin and only one or two layers are distinguishable. The fibers do not show any agglutinated or generally allochthonous material. This sponge taxon commonly shows asexual buds.

Palaeosmenospongia kejiaoensis n. gen, n. sp. Wu & Reitner

(Figure 3a-m and Figure 4a-c)

Etymology. The new species is named after the Kejiao section.

Type specimens. One complete specimen (BGEG KJ10301) is selected as holotype (Figure 4a). Other three specimens are selected as Paratype I (BGEG KJ10302; Figure 4b), Paratype II (BGEG KJ10303; Figure 4c), and Paratype III (BGEG KJ10314; Figure 3i).

Horizon and locality. The greenish to brownish calcareous mudstone of the lowest Luolou Formation (lower Griesbachian); the Kejiao section of Duanshan Town in

Huishui County, Guizhou Province, southwest China.

Remarks. This new type of fossil aspiculate keratose demosponge is currently unique and has no obvious relatives. The new species is differentiated from the well-known keratose demosponges of the family Vauxiidae Walcott, 1920 as the latter are tubular and often branched (Rigby, 1980; Yang et al., 2017; Luo et al., 2020). The fiber skeleton of that taxon consists of a very regular reticulate network and shows, normally, a polygonal space between the fibers which is not observed in the new taxon. The fiber skeleton of the Vauxiidae is normally formed by two layers, a dermal and a choanosomal one, which was not observed in the new taxon. The Vauxiidae are most likely related to the Verongida or Verongimorpha *sensu* Erpenbeck et al. (2012) the other large phylogenetic group of aspiculate demosponges. The chemical composition of the fiber skeleton of the Vauxiidae has a chitin composition (Ehrlich et al., 2013) which is known in the Verongimorpha and not from the newly erected phylogenetic group "Keratosa" which includes the Dictyoceratida and Dendroceratida (Erpenbeck et al., 2012). The fiber skeleton of this group is composed only of spongin, a complex compound of scleroproteins. The key chemical signals that can be identified as specific organic components have been lost, but the morphological characteristics are closer to those of modern spongin textures. The new sponge exhibits some morphological similarities with the Cambrian taxon *Crumillospongia*. However, this taxon has a spicular skeleton with affinities to *Hazellia* (Rigby and Collins, 2004), which is probably related to the Halichondrida; a taxon that is explicitly not a keratose demosponge. Considering the similarity of the fiber structure, especially the arrangement of thick primary and thinner secondary fibers (Figure 4), our new taxon is most probably related to the modern genus *Smenospongia* Wiedenmayer, 1977 (Figure 4d-g).

4.3 Redox interpretation

4.3.1 Elemental geochemistry

Both trace elemental proxies: V/Cr and V/ (V + Ni) ratios are employed to unravel redox changes across the end-Permian mass extinction in Kejiao. Most V/Cr ratios from the uppermost Permian are rather low, ranging from 1.23 to 1.70. The low values continue up into the lowest Triassic and there is a transition between bed 78 and bed 79. The V/Cr ratios from bed 78 to bed 85 range from 2.13 to 4.08, within the dysoxic window (Figure 2).

The V/ (V + Ni) ratios derived from the Permian samples range from 0.075 to 0.54 (averaging 0.36), and the curve rose gradually following the PTB. Except for two points that are lower, the V/ (V + Ni) ratios of the mudstone are greater than 0.84 (Figure 2), indicating euxinia (Hatch and Leventhal, 1992; Shi et al., 2016), which is reinforced by beds that consist of dark, organic-rich mudstone with fine, horizontal laminae (Fig. S4E-F). Thus, the sponge-bearing layers were most probably deposited in a basin with oxygen-poor condition.

4.3.2 Pyrite Framboid Analysis and Redox Interpretation

A total of 17 out of 22 (77%) samples yield pyrite framboids (Figure 2). Overall, the Lower Triassic yellowish mudstones tend to yield more abundant and smaller framboids than the uppermost Permian dark-colored siliceous mudstones. No framboids were found in the lowest Triassic greenish mudstone. Framboids derived from the six uppermost Permian samples have mean diameters (MD) of 7.15−8.96 μm with standard deviations (SD) of 2.28−3.65 μm, indicative of dysoxic conditions (Bond and Wignall, 2010; Figure S3). Eleven of the 16 Lower Triassic samples fall

within the anoxic field with MDs of 3.20−5.84 μm and SDs of 0.96−2.24 μm. Framboids from sponge-bearing horizons (Beds 82−84) all fall into the anoxic field (Figure 2; Figure S3). No framboids were found in Beds 73−78, which straddle the P−Tr boundary. These beds, containing ammonoids and bivalves, may represent a more oxic environment (Figure 2). The coeval oxygen-rich layers between two stages of anoxia also occur in the PTB beds at the GSSP in Meishan, South China and the Guryul Ravine section, Kashmir, India (Chen et al., 2015; Huang et al., 2017, 2018), suggesting that the redox history during the P−Tr transition was consistent with that elsewhere in the Paleo-Tethys region.

5 DISCUSSION

5.1 Taphonomy

The spongin skeletons of these soft-bodied sponges are well preserved, without any evidence of preferred orientation, deformation or lateral compression, suggesting *in situ* burial. Raman measurements show a high content of organic matter in the dark sponge remains (Figure 5), clearly distinguished from the surrounding matrix, indicating the high preservation potential for organic skeletons. Considering the morphological attributes, the preserved material is most likely to be the former spongin skeleton of an aspiculate demosponge.

Three factors are crucial for the exceptional preservation of these sponges. First is the preservation potential of the sponge skeleton. Unlike other soft tissues like epidermal cells, the spongin skeleton of keratose sponges is a tough material that is

nevertheless soft, elastic, absorbent, and insoluble in water and acids, and shows strong resistance to enzymatic degradation (Jesionowski et al., 2018). Second, high V/Cr and V/ (V + Ni) ratios from the sponge-bearing strata indicate dysoxic to anoxic conditions, which are considered as a prerequisite for the exceptional preservation of other Lagerstätten (e.g., Gaines et al., 2005, 2012). Third, in longitudinal section, the fossil-bearing mudstones have elongated silt-sized lenses embedded within a clay-rich dark matrix (Figure 6e-f), completely different from the underlying layers (Figure 6a-d). Flume experiments showed that such lenticular fabrics in shales originated from transport of surficial water-rich muds by currents (Schieber et al., 2010). Such lenticular fabrics were also found in other Lagerstätten (e.g., Gabbott et al., 2008, 2010). The slow-moving imbricated mud chips thus created a confined space, conducive to fossil preservation. Besides, this proves that the surrounding water was not stagnant.

5.2 Sponges after mass extinction event

The proliferation of the Kejiao sponges may have acted as a direct reflection of environmental deterioration after the end-Permian extinction. The sponges, together with tiny, thin-shelled brachiopods (Figure 3n-o) and few ammonoids, formed a typical sponge-dominated ecosystem (Figure 7) flourishing as opportunists in stressful environments. Keratose sponge fabrics found in PTB microbialites (Friesenbichler et al., 2018; Heindel et al., 2018; Baud et al., 2021; Chen et al., 2022; Wu et al., 2022a, b) are under discussion (Neuweiler et al. 2023). Luo et al. (2022), however, have

introduced a taphonomic concept which explains the preservation of complex spongin skeletons and related this to the assumptions made in Neuweiler et al. (2023). The Kejiao fauna provides first hard evidence that sponges proliferated after end-Permian mass extinction, confirming that survival ability of Keratosa, at least in deep-water settings. This study bridges the gap in our knowledge of sponges within the earliest Triassic and opens a limited window for incorporating sponges into the narrative surrounding post-extinction ecosystems. In addition, the proliferation of sponges after disaster events is a common phenomenon: e.g., end-Ordovician, Late Devonian, end-Triassic extinction events and modern El Niño events (Vishnevskaya et al., 2002; Delecat & Reitner, 2005; Delecat et al. 2011; Kelmo et al., 2013; Ritterbush et al., 2015; Li et al., 2015; Botting et al., 2017), suggesting that some sponges demonstrated remarkable resilience in adapting to and surviving in these extreme environmental conditions.

The P−Tr great dying was associated with several extreme environmental and climate upheavals, such as expanded marine anoxia (Zhang et al., 2018). In Kejiao, V/Cr ratio and taphonomic evidence indicate that the preservation facilitated by low levels of oxygen Lagerstätte-type sponges, suggested that they inhabited a relatively oxygen-poor environment. In fact, some modern demosponges can survive under low-oxygen conditions (Hoffmann et al. 2005; Mills et al., 2014) and, the earliest crown-group sponges had already evolved a great tolerance of oxygen-deficient habitats (Mills et al., 2014). The tolerance of low-oxygen conditions is also a property of the Cambrian Burgess-Shale-type sponge group (Gaines et al., 2005; Li et al.,

2021). Sponges have a proven tolerance of temperature and pH change (Duckworth et al., 2012; Kelmo et al., 2013), which would help survival of disruptive environmental change following the extinction event. Furthermore, sponges possess efficient filtration systems that ensure their survival in nutrient-depleted environments (Leys et al., 2011). Abundant keratose sponges occupied the post-extinction oxygen-depleted habitats in Kejiao and proliferated when most other marine animals suffered massive casualties. One or more of the above abilities were conducive to their survival in stressful environments and proliferate after catastrophic events.

5.3 The Ecological Function and Significance of Kejiao Sponge

The phylogenomic dataset available supports sponges at the base of the metazoan tree of life (Simion et al., 2017). The Ediacaran-Cambrian rise of sponges is believed to have played a role in the initiation of seawater oxygenation by redistributing organic carbon while oxygenating ambient environments through their ability to filter suspended organic matter from seawater, aiding the diversification of modern-type ecosystems (Chang et al., 2019; Zheng et al., 2022). Modern experiments show that sponges have the potential to support the whole ecosystem by transforming dissolved organic matter into particulate detritus that are beneficial for higher trophic levels (de Goeij et al., 2013), and this ecological role extends even to deep-sea environments (Bart et al., 2021). This ability positioned sponges as part of a highly efficient recycling pathway, allowing barren marine ecosystem develop high diversity (de Goeij et al., 2013). Additionally, modern studies demonstrate that sponge

caves could serve as refuges and ‘seed banks’ for nearby dwindling corals (Slattery et al., 2013), confirming the potential contribution of sponges in biotic recovery. Furthermore, the physical structure of sponge colonies could provide shelter and substrate for a diverse array of organisms, creating microhabitats that support the settlement and growth of numerous species (Chin et al., 2020).

In recent years, there has been a notable resurgence of scientific interest in sponges, driven by a growing recognition of their significant contributions to the biodiversity and functioning of marine ecosystems (Bell et al., 2018; Lesser and Slattery, 2020). Extensive research has yielded fresh insights into the pivotal role played by deep-water sponges (Rooks et al., 2020; Pierrejean et al., 2020). Modern investigations have found that deep-water sponge grounds could serve as reservoirs of biodiversity, creating habitats and refuges for other organisms (Hogg et al., 2010). And, keratose sponges have become the dominant species in some modern deep-sea habitats (Enrichetti et al., 2019), validating the adaptability and ecological potential of this group of sponges.

To sum up, there are some key examples that suggest that sponges acted as a prelude to highly diverse communities in early ecosystem evolution and following ecological crises. However, further research is needed to fully understand the extent of their role in these processes. The mechanism of how ecosystems began to recover during the Early Triassic is currently not well understood and the long-neglected sponge communities might also have participated in biogeochemical cycling in the earliest Triassic. The appearance of sponges in different facies after disaster events

implies that low-trophic-level ecosystems could have persisted in some environments, maintaining the original dynamic of biotic recovery, ready to drive the ecosystem to a higher level. Kejiao sponge assemblages represent a symbol of the collapse of marine ecosystem, but also have the potential to serve as a hotbed of marine life and the engine of the reboot of the marine ecosystem. Moreover, whether the proliferation of sponges is a local event or reached a global scale requires further investigation, which will help us better understand the ecological dynamics of the Early Triassic

6 CONCLUSIONS

Abundant keratose sponges occur in the lowest Triassic mudstone in a deep-water basin facies in Southwest China. The Kejiao sponge represents a remarkable taphonomic phenomenon with important implications for ecosystem evolution after major biotic crises. The new sponge is closest to the extant Dictyoceratida, and also exhibits a budding mode of asexual reproduction. The well-preserved fiber skeleton shows a centimeter-sized vase-shaped habit commonly with a central osculum. Sedimentary, taphonomic and trace elemental analyses show a low-oxygenated fossil Lagerstätte mode of preservation, and indicate the sponges proliferated in a deep-water, dysoxic to anoxic habitat, highlighting the high tolerance of these sponges. The first batch of sponges after disaster events may have contributed to the return of other sessile suspension feeders through their specialized ecological functions, and acted as ecosystem engineers driving biotic recovery after the

end-Permian extinction. It appears that further evaluation is warranted regarding the implications of the great dying for sponge taxa, as well as their subsequent Triassic evolution and ecological expansion.

ACKNOWLEDGMENTS

Both Li Xu and Wei Wang from School of Media Communications, China University of Geosciences (Wuhan) are thanked for drawing the artistic reconstruction (Figure 7) of the paper. Two anonymous reviewers are thanked for their critical comments and constructive suggestions that have greatly improved the quality of the paper. Harper thanks the Leverhulme Trust (UK) for support. Conny Hundertmark (Department of Geobiology, University of Göttingen) is greatly acknowledged for graphic interpretation of the new sponge taxon. This study is supported by NSFC grants (41930222).

REFERENCES CITED

Antcliffe, J. B., Callow, R. H., & Brasier, M. D. (2014). Giving the early fossil record of sponges a squeeze. Biological Reviews, 89(4), 972-1004. https://doi.org/10.1111/brv.12090

Bart, M. C., Hudspith, M., Rapp, H. T., Verdonschot, P. F., & De Goeij, J. M. (2021). A deep-sea sponge loop? Sponges transfer dissolved and particulate organic carbon and nitrogen to associated fauna. Frontiers in Marine Science, 8, 604879. https://doi.org/10.3389/fmars.2021.604879.

Baud, A., Richoz, S., Brandner, R., Krystyn, L., Heindel, K., Mohtat, T., Mohtat-Aghai, P., & Horacek, M. (2021). Sponge takeover from end-Permian mass extinction to Early Induan time: Records in Central Iran microbial buildups. Frontiers in Earth Science, 9, 586210. https://doi.org/10.3389/feart.2021.586210.

Bell, J. J., Rovellini, A., Davy, S. K., Taylor, M. W., Fulton, E. A., Dunn, M. R., Bennett, H. M., Kan & Webster, N. S. (2018). Climate change alterations to ecosystem dominance: how might sponge-dominated reefs function? Ecology, 99(9), 1920-1931. https://doi.org/10.1002/ecy.2446

Bergquist, P. (1978). Sponges. University of California Press, Los Angeles.

Bond, D. P. G., & Wignall, P. B. (2010). Pyrite framboid study of marine Permian–Triassic boundary sections: a complex anoxic event and its relationship to contemporaneous mass extinction. Geological Society of America Bulletin, 122(7-8), 1265-1279. https://doi.org/10.1130/B30042.1

Botting, J. P., Muir, L. A., Zhang, Y., Ma, X., Ma, J., Wang, L., Zhang, J., Song, Y., & Fang, X., (2017). Flourishing sponge-based ecosystems after the end-Ordovician mass extinction. Current Biology, 27(4), 556-562. https://doi.org/10.1016/j.cub.2016.12.061.

Burton, M. (1934). Sponges. Great Barrier Reef Expedition, 1928–29. Scientific Reports, 4(14), 513-621.

Brayard, A., Krumenacker, L. J., Botting, J. P., Jenks, J. F., Bylund, K. G., Fara, E., Vennin, E., Olivier, N., Goudemand, N., Saucède, T., Charbonnier, S., Romano, C., Doguzhaeva, L., Thuy, B., Hautmann, M., Stephen, D. A., Thomazo, C. &

411 Escarguel, G. (2017). Unexpected Early Triassic marine ecosystem and the rise
412 of the Modern evolutionary fauna. Science Advances, 3(2), e1602159.
413 https://doi.org/10.1126/sciadv.1602159
414 Chang, S., Zhang, L., Clausen, S., Bottjer, D. J., & Feng, Q. (2019). The
415 Ediacaran-Cambrian rise of siliceous sponges and development of modern oceanic
416 ecosystems. Precambrian Research, 333, 105438.
417 https://doi.org/10.1016/j.precamres.2019.105438.
418 Chen, Z. Q., & Benton, M. J. (2012). The timing and pattern of biotic recovery
419 following the end-Permian mass extinction. Nature Geoscience, 5(6), 375-383.
420 https://doi.org/10.1038/ngeo1475.
421 Chen, Z. Q., Shi, G. R., & Kaiho, K. (2002). A new genus of rhynchonellid
422 brachiopod from the Lower Triassic of South China and implications for timing the
423 recovery of Brachiopoda after the end-Permian mass extinction. Palaeontology,
424 45(1), 149-164. https://doi.org/10.1111/1475-4983.00231
425 Chen, Z. Q., Yang, H., Luo, M., Benton, M. J., Kaiho, K., Zhao, L. S., Huang, Y. G.,
426 Zhang, K. X., Fang, Y. H., Jiang, H. S., Qiu, H., Li, Y., Tu, C. Y., Shi, L., Zhang, L.,
427 Feng, X. Q., & Chen, L. (2015). Complete biotic and sedimentary records of the
428 Permian–Triassic transition from Meishan section, South China: ecologically
429 assessing mass extinction and its aftermath. Earth-Science Reviews, 149, 67-107.
430 https://doi.org/10.1016/j.earscirev.2014.10.005
431 Chen, Z. Q., Fang, Y. H., Wignall, P. B., Guo, Z., Wu, S. Q., Liu, Z. L., Wang, R. Q.,
432 Huang, Y. G., & Feng, X. Q. (2022). Microbial blooms triggered pyrite framboid

enrichment and oxygen depletion in carbonate platforms immediately after the latest Permian extinction. Geophysical Research Letters, 49(7), e2021GL096998. https://doi.org/10.1029/2021GL096998

Chin, Y. Y., Prince, J., Kendrick, G., & Abdul Wahab, M. A. (2020). Sponges in shallow tropical and temperate reefs are important habitats for marine invertebrate biodiversity. Marine Biology, 167(11), 164. https://doi.org/10.1007/s00227-020-03771-1

Dai, X., Davies, J. H., Yuan, Z., Brayard, A., Ovtcharova, M., Xu, G. H., Liu, X. K., Smith, C. P. A., Schweitzer, C. E., Li, M. T., Perrot, M. G., Jiang, S. Y., Miao, L. Y., Cao, Y. R., Yan, J., Bai, R. Y., Wang, F. Y., Guo, W., Song, H. Y., Tian, L., Corso, J. D., Liu, Y. T., Chu, D. L., & Song, H. (2023). A Mesozoic fossil lagerstätte from 250.8 million years ago shows a modern-type marine ecosystem. Science, 379(6632), 567-572. https://doi.org/10.1126/science.adf1622

Delecat, S., & Reitner, J. (2005). Sponge communities from the Lower Liassic of Adnet (Northern Calcareous Alps). Facies, 51, 385-404. https://doi.org/10.1007/s10347-005-0045-x

Delecat, S., Arp, G., & Reitner, J. (2011). Aftermath of the Triassic–Jurassic Boundary Crisis: Spiculite Formation on drowned Triassic steinplatte reef-slope by communities of hexactinellid sponges (Northern Calcareous Alps, Austria). In: Reitner, J., Queric, N.-V., & Arp, G. (eds), Advances in Stromatolite Geobiology. Lecture Notes in Earth Sciences, 131, 355-390. https://doi.org/10.1007/978-3-642-10415-2_23

De Goeij, J. M., Van Oevelen, D., Vermeij, M. J., Osinga, R., Middelburg, J. J., De Goeij, A. F., & Admiraal, W. (2013). Surviving in a marine desert: the sponge loop retains resources within coral reefs. Science, 342(6154), 108-110. https://doi.org/10.1126/science.1241981.

Duckworth, A. R., West, L., Vansach, T., Stubler, A., & Hardt, M. (2012). Effects of water temperature and pH on growth and metabolite biosynthesis of coral reef sponges. Marine Ecology Progress Series, 462, 67-77. https://doi.org/10.3354/meps09853.

Ehrlich, H., Rigby, J. K., Botting, J., Tsurkan, M., Werner, C., Schwille, P., Petrášek, Z., Pisera, A., Simon, P., & Sivkov, V. (2013). Discovery of 505-million-year old chitin in the basal demosponge *Vauxia gracilenta*. Scientific Reports, 3(1), 3497. https://doi.org/10.1038/srep03497

Enos, P., Lehrmann, D. J., Jiayong, W., Youyi, Y., Jiafei, X., Chaikin, D. H., Minzoni, M., Berry, A. K., & Montgomery, P., (2006). Triassic evolution of the Yangtze platform in Guizhou Province, People's Republic of China, Geological Society of America, Boulder.

Enrichetti, F., Bavestrello, G., Betti, F., Coppari, M., Toma, M., Pronzato, R., Canese, S., Bertolino, M., Costa, G., Pansini, M., & Bo, M. (2020). Keratose-dominated sponge grounds from temperate mesophotic ecosystems (NW Mediterranean Sea). Marine Ecology, 41(6), e12620. https://doi.org/10.1111/maec.12620

Erpenbeck, D., Sutcliffe, P., Cook, S. D. C., Dietzel, A., Maldonado, M., van Soest, R. W., Hooper, J. N., & Wörheide, G. (2012). Horny sponges and their affairs: On the

phylogenetic relationships of keratose sponges. Molecular Phylogenetics and Evolution, 63(3), 809-816. https://doi.org/10.1016/j.ympev.2012.02.024

Ferrari, A. C., & Robertson, J. (2000). Interpretation of Raman spectra of disordered and amorphous carbon. Physical review B, 61(20), 14095. https://doi.org/10.1103/PhysRevB.61.14095.

Finks, R. M. (2010). Hypercalcified demosponges and the end-Permian extinction. Global and Planetary Change, 73(1-2), 141-148. https://doi.org/10.1016/j.gloplacha.2010.03.009.

Friesenbichler, E., Richoz, S., Baud, A., Krystyn, L., Sahakyan, L., Vardanyan, S., Peckmann, J., Reitner, J., & Heindel, K. (2018). Sponge-microbial build-ups from the lowermost Triassic Chanakhchi section in southern Armenia: Microfacies and stable carbon isotopes. Palaeogeography, Palaeoclimatology, Palaeoecology, 490, 653-672. https://doi.org/10.1016/j.palaeo.2017.11.056.

Gabbott, S. E., Zalasiewicz, J., & Collins, D. (2008). Sedimentation of the phyllopod bed within the Cambrian Burgess Shale Formation of British Columbia. Journal of the Geological Society, 165(1), 307-318.

Gabbott, S. E., Zalasiewicz, J., Aldridge, R. J., & Theron, J. N. (2010). Eolian input into the Late Ordovician postglacial Soom Shale, South Africa. Geology, 38(12), 1103-1106. https://doi.org/10.1130/G31426.1.

Gaines, R. R., Hammarlund, E. U., Hou, X., Qi, C., Gabbott, S. E., Zhao, Y., Peng, J., & Canfield, D. E. (2012). Mechanism for Burgess Shale-type preservation. Proceedings of the National Academy of Sciences, United States of America,

109(14), 5180-5184. https://doi.org/10.1073/pnas.1111784109

Gaines, R. R., Kennedy, M. J., & Droser, M. L. (2005). A new hypothesis for organic preservation of Burgess Shale taxa in the middle Cambrian Wheeler Formation, House Range, Utah. Palaeogeography, Palaeoclimatology, Palaeoecology, 220(1-2), 193-205. https://doi.org/10.1016/j.palaeo.2004.07.034.

Gaino, E., Scalera Liaci, L., Sciscioli, M., & Corriero, G. (2006). Investigation of the budding process in Tethya citrina and Tethya aurantium (Porifera, Demospongiae). Zoomorphology, 125(2), 87. https://doi.org/10.1007/s00435-006-0015-z.

Grant, R. E., & Todd, R. B. (1836). Animal Kingdom. The Encyclopaedia of Anatomy and Physiology, 1, 107-118.

Guo, Z., Chen, Z. Q., Harper, D. A. T., & Huang, Y. G. (2022). Permian–Triassic phylogenetic and morphologic evolution of rhynchonellide brachiopods. Paleobiology, 48(1), 99-119. https://doi.org/10.1017/pab.2021.25

Harper, D. A.T., Hammarlund, E. U., Topper, T. P., Nielsen, A. T., Rasmussen, J. A., Park, T. Y. S., & Smith, M. P. (2019). The Sirius Passet Lagerstätte of North Greenland: a remote window on the Cambrian explosion. Journal of the Geological Society, 176(6), 1023-1037. https://doi.org/10.1144/jgs2019-043.

Hatch, J. R., & Leventhal, J. S. (1992). Relationship between inferred redox potential of the depositional environment and geochemistry of the Upper Pennsylvanian (Missourian) Stark Shale Member of the Dennis Limestone, Wabaunsee County, Kansas, USA. Chemical Geology, 99(1-3), 65-82. https://doi.org/10.1016/0009-2541(92)90031-Y.

He, Z. L., Li, S. J., Li, Y. Q., & Gao, J. (2022). Multi-directional and multiphase tectonic modification, and hydrocarbon differential enrichment in the iddle-Upper Yangtze Region. Journal of Earth Science, 33(5), 1246–1259. https://doi.org/10.1007/s12583-022-1738-6

Heindel, K., Foster, W. J., Richoz, S., Birgel, D., Roden, V. J., Baud, A., Brandner, R., Krystyn, L., Mohtat, T., Koşun, E., Twitchett, J. R., Reitner, J., & Peckmann, J. (2018). The formation of microbial-metazoan bioherms and biostromes following the latest Permian mass extinction. Gondwana Research, 61, 187-202. https://doi.org/10.1016/j.gr.2018.05.007

Hogg, M. M., Tendal, O. S., Conway, K. W., Pomponi, S. A., Van Soest, R. W. M., Gutt, J., Krautter, M., & Roberts, J. M. (2010). Deep-sea sponge grounds: reservoirs of biodiversity. UNEP-WCMC Biodiversity Series, 32, 1-86.

Hoffmann, F., Larson, O., Thiel, V., Rapp, H. T., Pape, T., Michaelis, W., & Reitner, J. (2005). An anaerobic world in sponges. Geomicrobiology Journal, 22, 1-10. https://doi.org/10.1080/01490450590922505

Huang, Y. G., Chen, Z. Q., Wignall, P. B., & Zhao, L. (2017). Latest Permian to Middle Triassic redox condition variations in ramp settings, South China: Pyrite framboid evidence. Geological Society of America Bulletin, 129(1-2), 229-243. https://doi.org/10.1130/B31458.1

Huang, Y. G., Chen, Z. Q., Algeo, T. J., Zhao, L., Baud, A., Bhat, G. M., Zhang, L., & Guo, Z. (2019). Two-stage marine anoxia and biotic response during the Permian–Triassic transition in Kashmir, northern India: pyrite framboid evidence.

543 Global and Planetary Change, 172, 124-139.
544 https://doi.org/10.1016/j.gloplacha.2018.10.002
545 Huang, Y., Chen, Z. Q., Roopnarine, P. D., Benton, M. J., Zhao, L., Feng, X., & Li, Z.
546 (2023). The stability and collapse of marine ecosystems during the
547 Permian-Triassic mass extinction. Current Biology, 33(6), 1059-1070.
548 https://doi.org/10.1016/j.cub.2023.02.007
549 Jesionowski, T., Norman, M., Żółtowska-Aksamitowska, S., Petrenko, I., Joseph, Y.,
550 & Ehrlich, H. (2018). Marine spongin: Naturally prefabricated 3D scaffold-based
551 biomaterial. Marine Drugs, 16(3), 88. https://doi.org/10.3390/md16030088.
552 Jiang, Y., Wu, H. T., Xiao, Y. F., Yang, T. L., He, W. H., Wang, H., Sun, X., & Wu, S.
553 B. (2018), Ammonoid zonations of Permian-Triassic boundary strata from Kejiao
554 section, Huishui County, southern Guizhou Province, South China and regional
555 correlatio: Geological Science and Technolgical Inforation, 37, 65-73.
556 https://doi.org/10.19509/j.cnki.dzkq.2018.0608.
557 Jing, Y. H., Chen, Z. Q., & Tu, C. Y. (2022). A late Paleoproterozoic microfossil
558 community from siliceous granules, Dahongyu Formation, North China.
559 Precambrian Research, 377, 106723.
560 https//doi.org/10.1016/j.precamres.2022.106723.
561 Jones, B., & Manning, D. A. (1994). Comparison of geochemical indices used for the
562 interpretation of palaeoredox conditions in ancient mudstones. Chemical geology,
563 111(1-4), 111-129. https://doi.org/10.1016/0009-2541(94)90085-X.
564 Kelmo, F., Bell, J. J., & Attrill, M. J. (2013). Tolerance of sponge assemblages to

565 temperature anomalies: resilience and proliferation of sponges following the
566 1997–8 El-Nino southern oscillation. PLoS One, 8(10), e76441.
567 https://doi.org/10.1371/journal.pone.0076441.
568 Lee, J. H., & Riding, R. (2021). The ‘classic stromatolite’ *Cryptozoön* is a keratose
569 sponge-microbial consortium. Geobiology, 19(2), 189-198.
570 https://doi.org/10.1111/gbi.12422
571 Lee, J. H., & Riding, R. (2023). Recognizing sponge in *Spongiostroma* Gürich, 1906
572 from the Mississippian of Belgium. Journal of Paleontology, 97(1), 26-37.
573 https://doi.org/10.1017/jpa.2022.73
574 Lehrmann, D. J., Payne, J. L., Felix, S. V., Dillett, P. M., Wang, H., Yu, Y., & Wei, J.
575 (2003). Permian–Triassic boundary sections from shallow-marine carbonate
576 platforms of the Nanpanjiang Basin, South China: implications for oceanic
577 conditions associated with the end-Permian extinction and its aftermath. Palaios,
578 18(2), 138-152.
579 https://doi.org/10.1669/0883-1351(2003)18<138:PBSFSC>2.0.CO;2.
580 Lesser, M. P., & Slattery, M. (2020). Will coral reef sponges be winners in the
581 Anthropocene?. Global Change Biology, 26(6), 3202-3211.
582 https://doi.org/10.1111/gcb.15039
583 Leys, S. P., Yahel, G., Reidenbach, M. A., Tunnicliffe, V., Shavit, U., & Reiswig, H.
584 M. (2011). The sponge pump: the role of current induced flow in the design of the
585 sponge body plan. PloS one, 6(12), e27787.
586 https://doi.org/10.1371/journal.pone.0027787

Li, L., Feng, H., Janussen, D., & Reitner, J. (2015). Unusual deep water sponge assemblage in South China—witness of the end-Ordovician mass extinction. Scientific Reports, 5, 16060. https://doi.org/10.1038/srep16060.

Li, Z. H., Zhang, M., Chen, Z. Q., Algeo, T. L., Zhao, L. S., & Zhang, F. F. (2021). Early Cambrian oceanic oxygenation and evolution of early animals: A critical review from the South China Craton. Global and Planetary Change, 204, 103561. https//doi.org/10.1016/j.gloplacha.2021.103561

Luo, C., & Reitner, J. (2014). First report of fossil "keratose" demosponges in Phanerozoic carbonates: preservation and 3-D reconstruction. Naturwissenschaften, 101, 467-477. https://doi.org/10.1007/s00114-014-1176-0.

Luo, C., Pei, Y., Richoz, S., Li, Q., and Reitner, J., 2022, Identification and current palaeobiological understanding of "Keratosa"-type nonspicular demosponge fossils in carbonates: with a new example from the lowermost Triassic, Armenia. Life, 12, 1348. https://doi.org/10.3390/life12091348.

Luo, C., Zhao, F., & Zeng, H. (2020). The first report of a vauxiid sponge from the Cambrian Chengjiang Biota. Journal of Paleontology, 94(1), 28-33. https://doi.org/10.1017/jpa.2019.52.

Mills, D. B., Ward, L. M., Jones, C., Sweeten, B., Forth, M., Treusch, A. H., & Canfield, D. E. (2014). Oxygen requirements of the earliest animals. Proceedings of the National Academy of Sciences, United States of America, 111(11), 4168-4172. https://doi.org/10.1073/pnas.1400547111.

Minchin, E. A., & Lankester, E. R. (1900). Chapter III. Sponges. A Treatise on

609 Zoology. Part II. The Porifera and Coelenterata, 2, 1-178.Neuweiler, F., Kershaw,
610 S., Boulvain, F., Matysik, M., Sendino, C., McMenamin, M., & Munnecke, A.
611 (2023). Keratose sponges in ancient carbonates – A problem of interpretation.
612 Sedimentology, 70, 927-968. https://doi.org/10.1111/sed.13059
613 Pierrejean, M., Grant, C., Neves, B. D. M., Chaillou, G., Edinger, E., Blanchet, F. G.,
614 Maps, F., Nozais, C., & Archambault, P. (2020). Influence of deep-water corals and
615 sponge gardens on infaunal community composition and ecosystem functioning in
616 the Eastern Canadian Arctic. Frontiers in Marine Science, 7, 495.
617 https://doi.org/10.3389/fmars.2020.00495
618 Rigby, J. K. (1980). The new Middle Cambrian sponge *Vauxia magna* from the
619 Spence Shale of northern Utah and taxonomic position of the Vauxiidae. Journal of
620 Paleontology, 54, 234-240.
621 Rigby, J.K., & Collins, D. (2004). Sponges of the Middle Cambrian Burgess Shale
622 and Stephen Formations, British Columbia. Toronto, Royal Ontario Museum,
623 1-155.
624 Ritterbush, K. A., Rosas, S., Corsetti, F. A., Bottjer, D. J., & West, A. J. (2015).
625 Andean sponges reveal long-term benthic ecosystem shifts following the
626 end-Triassic mass extinction. Palaeogeography, Palaeoclimatology, Palaeoecology,
627 420, 193-209. https://doi.org/10.1016/j.palaeo.2014.12.002.
628 Rooks, C., Fang, J. K. H., Mørkved, P. T., Zhao, R., Rapp, H. T., Xavier, J. R., &
629 Hoffmann, F. (2020). Deep-sea sponge grounds as nutrient sinks: denitrification is
630 common in boreo-Arctic sponges. Biogeosciences, 17(5), 1231-1245.

https://doi.org/10.5194/bg-17-1231-2020

Schieber, J., Southard, J. B., & Schimmelmann, A. (2010). Lenticular shale fabrics resulting from intermittent erosion of water-rich muds—interpreting the rock record in the light of recent flume experiments. Journal of Sedimentary Research, 80(1), 119-128. https://doi.org/10.2110/jsr.2010.005.

Scotese, C. R., (2014). Paleomap Project: Early Triassic Paleomap. Updated at: https://www.scotese.com/newpage8.htm

Shen, S. Z., Fan, J. X., Wang, X. D., Zhang, F. F., Shi, Y. K., & Zhang, S. H. (2022). How to build a high-resolution digital geological timeline? Journal of Earth Science, 33, 1629-1632. https://doi.org/10.1007/s12583-022-1315-z

Shi, L., Feng, Q. L., Shen, J., Ito, T., & Chen, Z. Q. (2016). Proliferation of shallow-water radiolarians coinciding with enhanced oceanic productivity in reducing conditions during the Middle Permian, South China: evidence from the Gufeng Formation of western Hubei Province. Palaeogeography, Palaeoclimatology, Palaeoecology, 444, 1-14. https://doi.org/10.1016/j.palaeo.2015.11.031

Simion, P., Philippe, H., Baurain, D., Jager, M., Richter, D. J., Di Franco, A., Roure, B., Satoh, N., Quéinnec, É., & Ereskovsky, A. (2017). A large and consistent phylogenomic dataset supports sponges as the sister group to all other animals. Current biology, 27(7), 958-967. https://doi.org/10.1016/j.cub.2017.02.031.

Slattery, M., Gochfeld, D. J., Easson, C. G., & O'Donahue, L. R. (2013). Facilitation of coral reef biodiversity and health by cave sponge communities. Marine Ecology

653 Progress Series, 476, 71-86. https://doi.org/10.3354/meps10139.
654 Sollas, W. (1875). Sponges *in* Encyclopaedia Britannica, ninth edition. London.
655 Sun, W. D., & Zhang, L. P. (2022). Preface: Pacific plate subduction and the
656 Yanshanian movement in Eastern China. Journal of Earth Science, 33(3), 541–543.
657 https://doi.org/10.1007/s12583-022-1311-3
658 Turner, E. C. (2021). Possible poriferan body fossils in early Neoproterozoic
659 microbial reefs. Nature, 596(7870), 87-91.
660 https://doi.org/10.1038/s41586-021-03773-z.
661 Velledits, F. (2008). Evolution of the Triassic reef communities. Hantkeniana, 6, 9-16.
662 Vishnevskaya, V., Pisera, A., & Racki, G. (2002). Siliceous biota [radiolarians and
663 sponges] and the Late Devonian biotic crisis: The Polish reference. Acta
664 Palaeontologica Polonica, 47(2), 211-226.
665 Walcott, C. D. (1920). Cambrian Geology and Paleontology: Middle Cambrian
666 Spongia, Smithsonian Institution.
667 Wang, H., He, W. H., Xiao, Y. F., Yang, T. L., Zhang, K. X., Wu, H. T., Huang, Y.F.,
668 Peng, X. F., & Wu, S. B. (2023). Stagewise collapse of biotic communities and its
669 relations to oxygen depletion along the north margin of Nanpanjiang Basin during
670 the Permian–Triassic transition. Palaeogeography, Palaeoclimatology,
671 Palaeoecology, 621, 111569. https://doi.org/10.1016/j.palaeo.2023.111569
672 Wiedenmayer, F. (1977). Shallow-water sponges of the western Bahamas: Experientia
673 Supplementum, 1-287.
674 Wu, S. Q., Chen, Z. Q., Su, C. M., Fang, Y. H., & Yang, H. (2022a). Keratose sponge

675 fabrics from the lowermost Triassic microbialites in South China: Geobiologic
676 features and Phanerozoic evolution. Global and Planetary Change, 211, 103787.
677 https://doi.org/10.1016/j.gloplacha.2022.103787.
678 Wu, S. Q., Chen, Z. Q., Fang, Y. H., Pei, Y., & Foster, W. J. (2022b). Benthic
679 Pleurocapsales (cyanobacteria) blooms catalyzing carbonate precipitation and
680 dolomitization following the end-Permian mass extinction. Geophysical Research
681 Letters, 49, e2022GL100819. https://doi.org/10.1029/2022GL100819
682 Yang, X., Zhao, Y., Babcock, L. E., & Peng, J. I. N. (2017). A new vauxiid sponge
683 from the Kaili Biota (Cambrian Stage 5), Guizhou, South China. Geological
684 Magazine, 154(6), 1334-1343. 10.1017/S0016756816001229.
685 Yin, H. F., Zhang, K. X., Tong, J. N., Yang, Z. Y., & Wu, S. B. (2001). The global
686 stratotype section and point (GSSP) of the Permian-Triassic boundary. Episodes,
687 24(2), 102-114. https://doi.org/10.18814/epiiugs/2001/v24i2/004
688 Zea, S., Henkel, T. P., & Pawlik, J.R. (2014). The Sponge Guide: A Picture Guide to
689 Caribbean Sponges. Available online at www.spongeguide.org.
690 Zhang, F. F., Algeo, T. J., Romaniello, S. J., Cui, Y., Zhao, L., Chen, Z. Q., & Anbar,
691 A. D. (2018). Congruent Permian-Triassic $\delta^{238}U$ records at Panthalassic and
692 Tethyan sites: Confirmation of global-oceanic anoxia and validation of the
693 U-isotope paleoredox proxy. Geology, 46(4), 327-330.
694 https://doi.org/10.1130/G39695.1.
695 Zheng, S., Feng, Q., van de Velde, S., Chang, S., Zhang, L., & Gao B. (2022).
696 Microfossil assemblages and indication of the source and preservation pattern of

organic matter from the Early Cambrian in South China. Journal of Earth Science, 33(3), 802–819. https://doi.org/10.1007/s12583-020-1117-0

FIGURE CAPTIONS

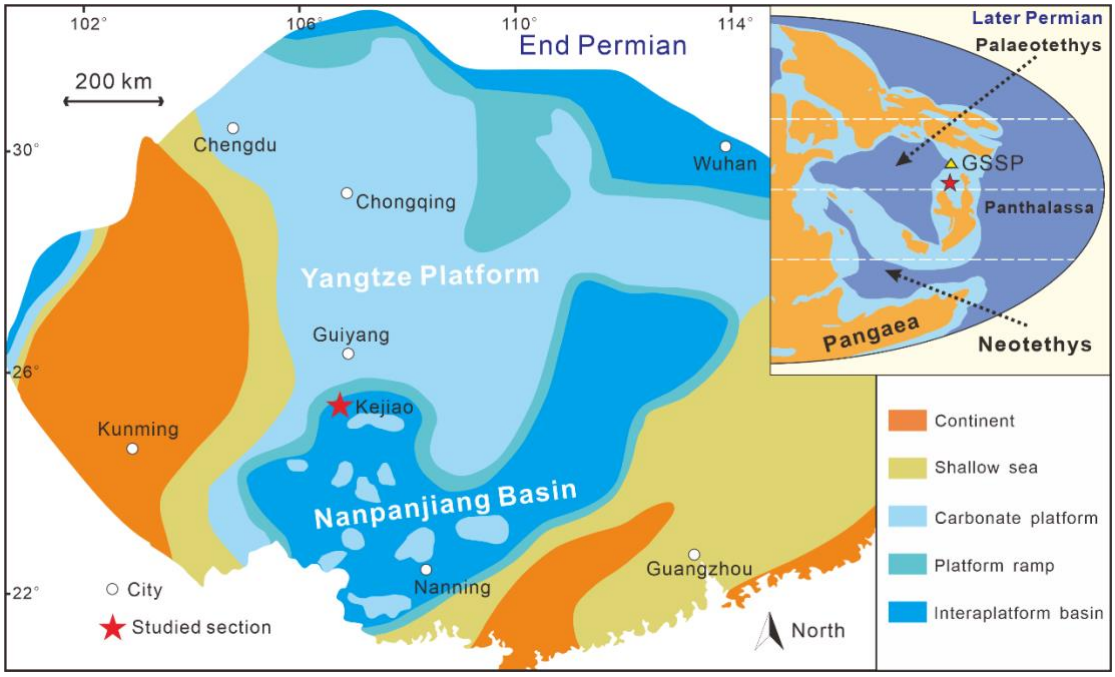

Figure 1 The later Permian paleogeographic map of the Paleo-Tethys (Scotese, 2014) and South China (Enos et al., 2006; Sun & Zhang, 2022) showing the site of the Kejiao section.

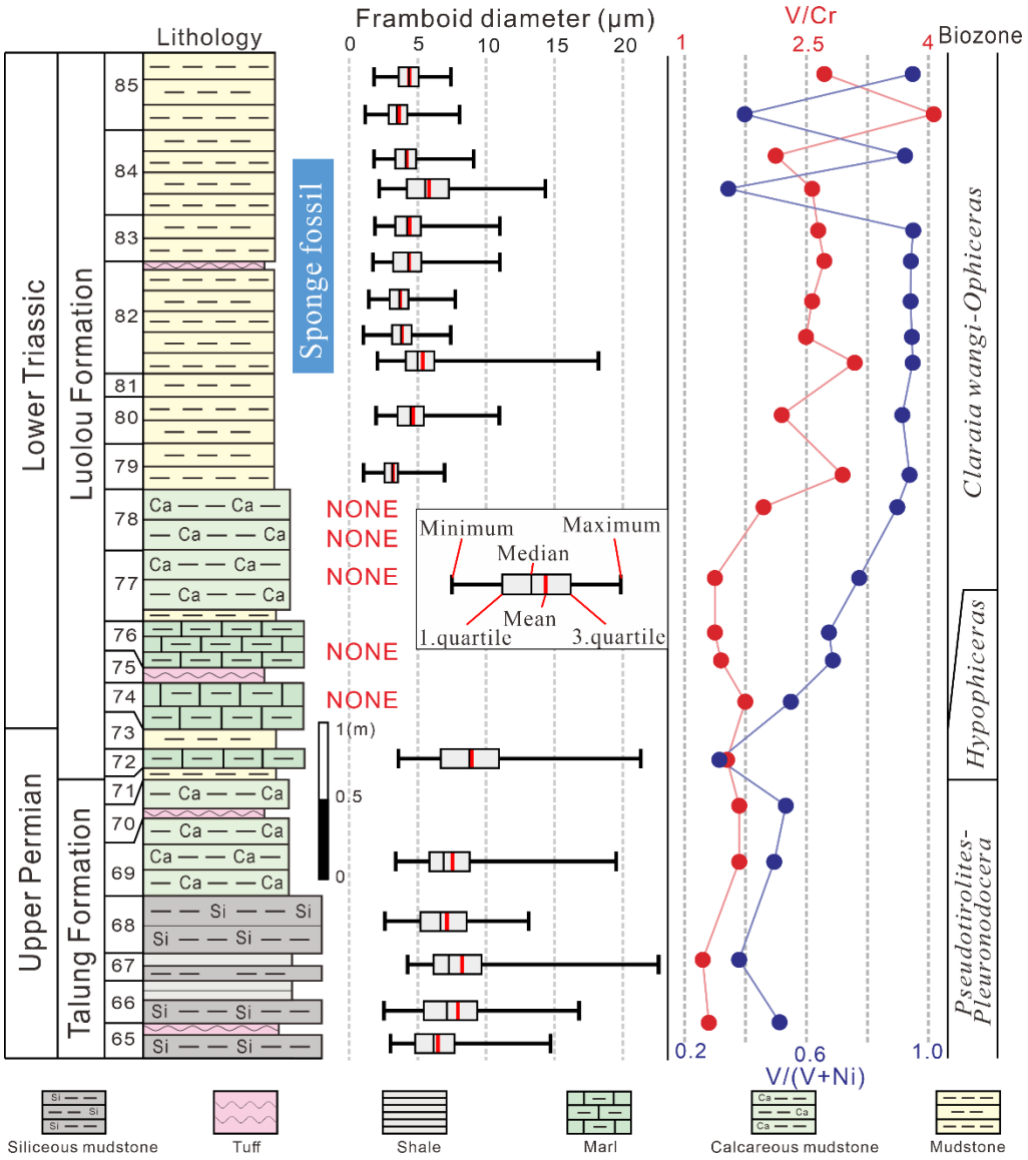

707 **Figure 2** The P−Tr boundary succession exposed at Kejiao showing lithology, fossil

708 distribution, pyrite framboid size distributions, and trace element ratios.

709

710

711

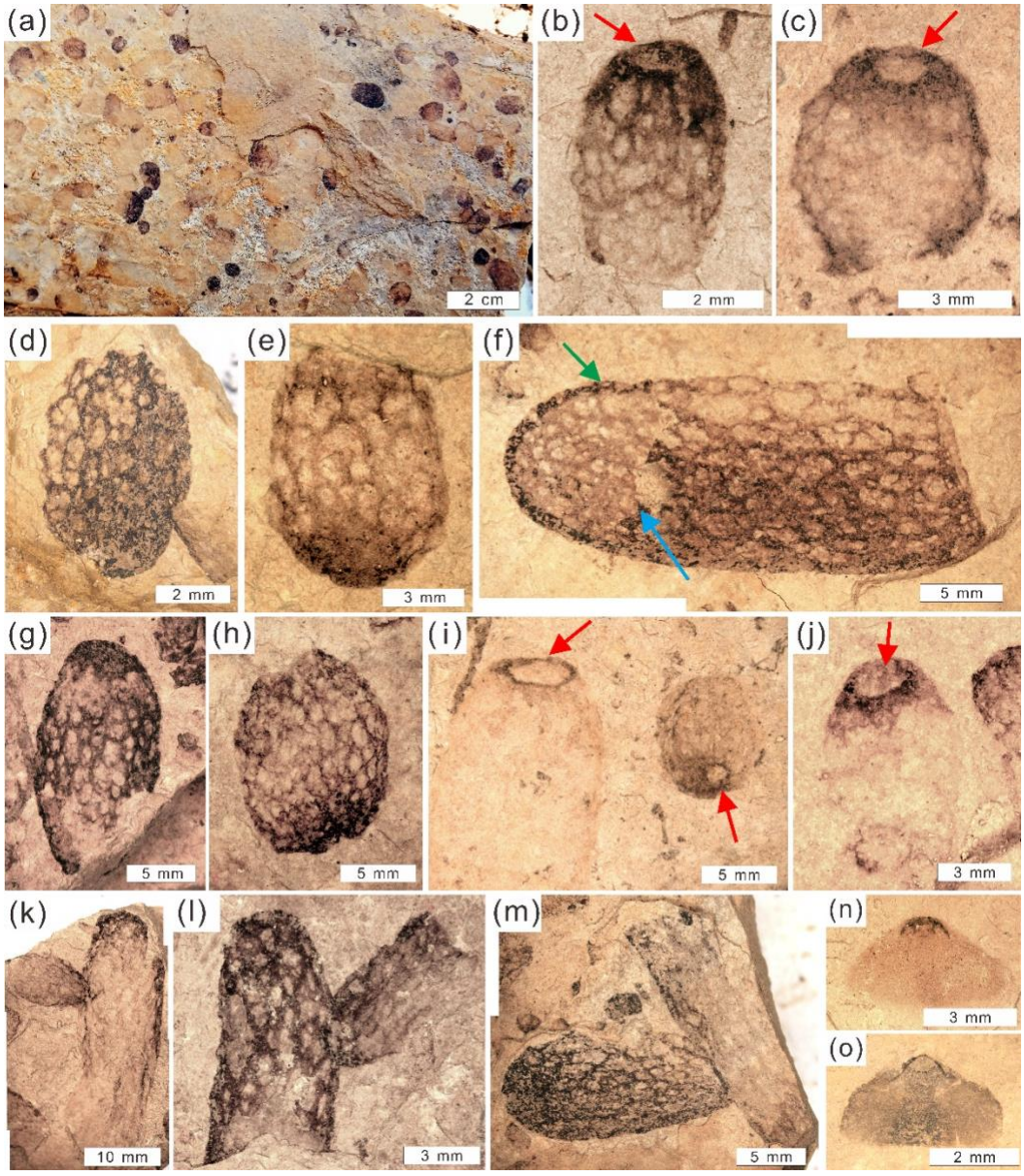

Figure 3 Selected specimens of the sponge and brachiopod fossils from the lowest Triassic in the Kejiao section. (a) Distribution of sponge fossils on the bedding surface. (b-j) Selected sponge specimens, red arrows point out the oscula (BGEG KJ10304-10313). (f) A broken specimen (BGEG KJ10305) showing thickened walls (green arrow) and interior view of intake network (blue arrow). (k-m) Branching sponges (BGEG KJ10314-10316, Paratype III) indicating a budding model of reproduction. (n-o) Brachiopod *Meishanorhynchia* shells associated with sponges on the same slab.

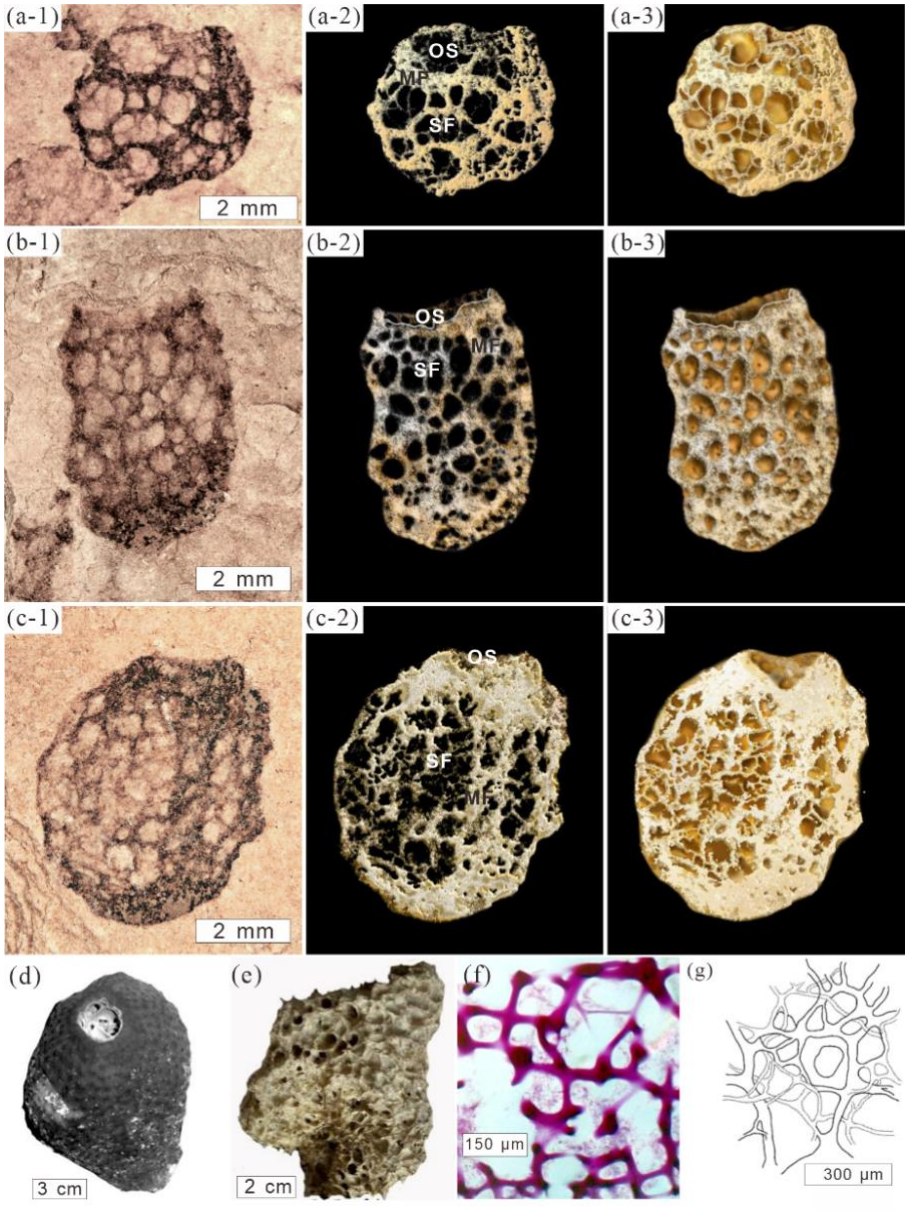

721

722 **Figure 4.** Fossil keratose sponges and their modern analogues. (a) A complete

723 specimen (BGEG KJ10301; Holotype) in optical microscopic view (a-1) and

724 reconstructions (a-2; a-3). (b) A complete specimen (BGEG KJ10302; Paratype I) in

725 optical microscopic view (b-1) and reconstructions (b-2; b-3). (c) A complete

726 specimen (BGEG KJ10303; Paratype II) (c-1), reconstructions (c-2; c-3). (a-2, b-2,

727 c-2) are directly extracted image and (a-3, b-3, c-3) are 3D reconstructions. OS =

728 osculum, MF = primary fiber, SF = secondary fiber. (d) *Smenospongia conulosa*

729 Pulizer-Finali, 1986; picture modified after *The Sponge Guide (Zea et al., 2014)*. (e)

Smenospongia sp., dried specimen. (f) Stained spongin skeleton of *Smenospongia* sp. showing thick primary and thin secondary fibers. (g) Drawing of the fiber skeleton of *Smenospongia conulosa*; modified after *The Sponge Guide* (Zea et al., 2014).

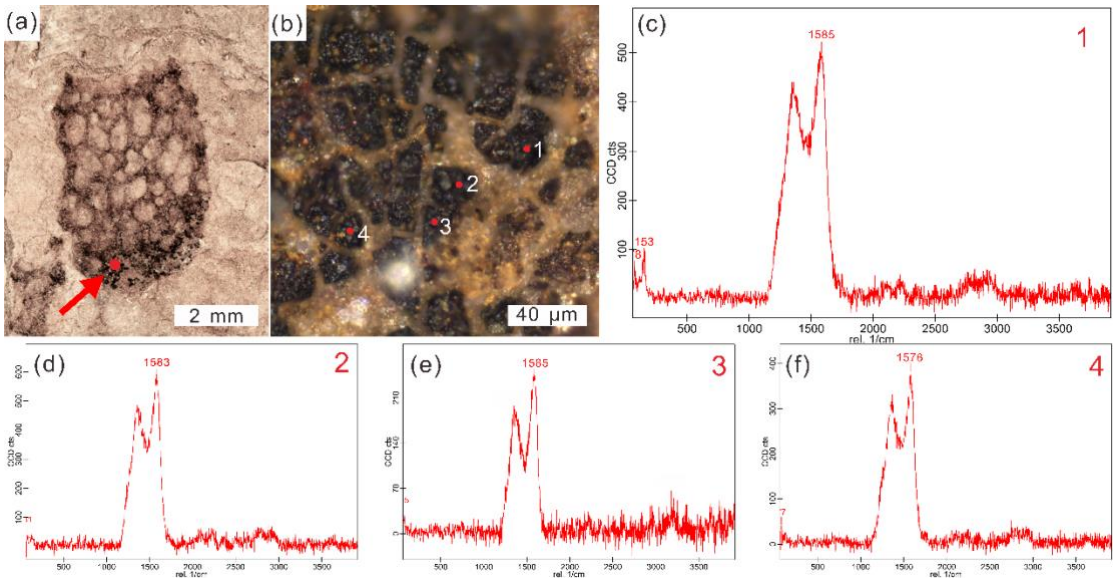

Figure 5 (a) Selected sponge fossil (BGEG KJ10302) for Raman spectrum analysis. (b) Close-up of the dark sponge remains in (a) marked with Raman spectrum points 1-4. (c-f) Raman spectrum of points 1-4.

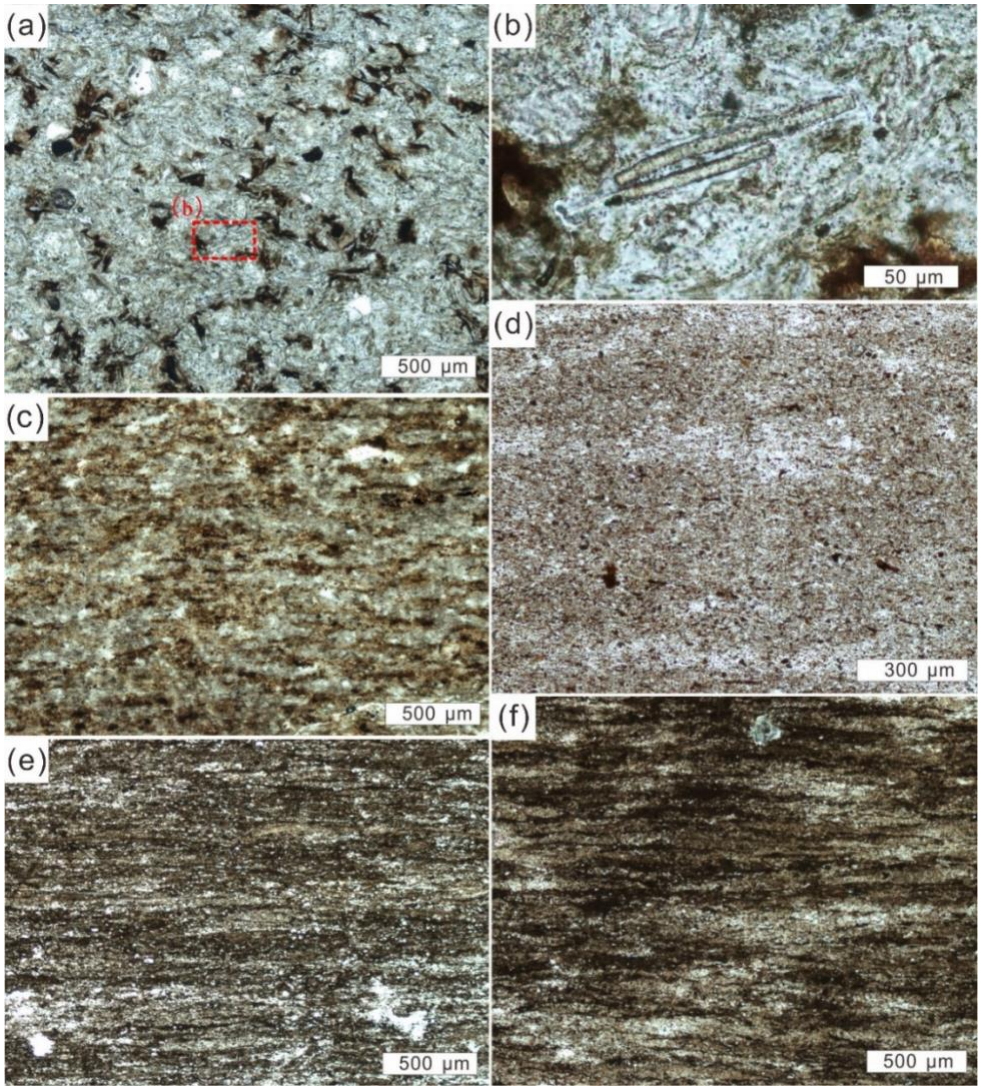

Figure 6 Microphotographs showing microfacies of the lowest Triassic strata in the Kejiao section. (a) Siliceous rock containing abundant sponge spicules (bed 65). (b) Close-up of boxed area in a showing details of sponge spicules. (c) Calcareous mudstone with oriented mineral arrangement (bed 69). (d) Slightly oriented Mineral arrangement (bed 81). (e) Horizontal bedding (bed 82). (f) Horizontal bedding (Bed 85).

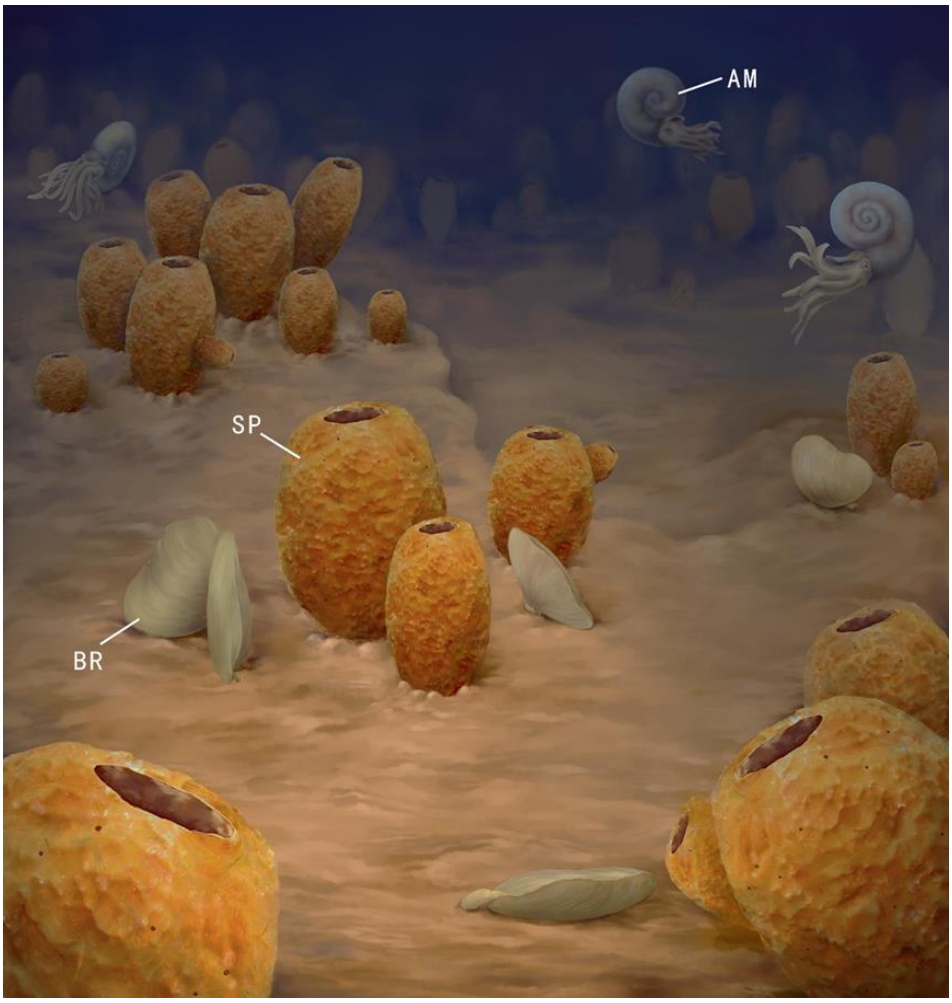

Figure 7 Artistic reconstruction of the marine ecosystem immediately after the end-Permian mass extinction in Kejiao section showing abundant keratose sponges and associated brachiopods and ammonoids. SP = sponge, BR = brachiopod, AM = ammonoid.

Supplemental Material for

New keratose sponges after the end-Permian extinction provide insights into biotic recoveries

Siqi Wu[1, 2], Joachim Reitner[3]*, Zhong-Qiang Chen[2] *, David A. T. Harper[2, 4], and Jianxin Yu[2]

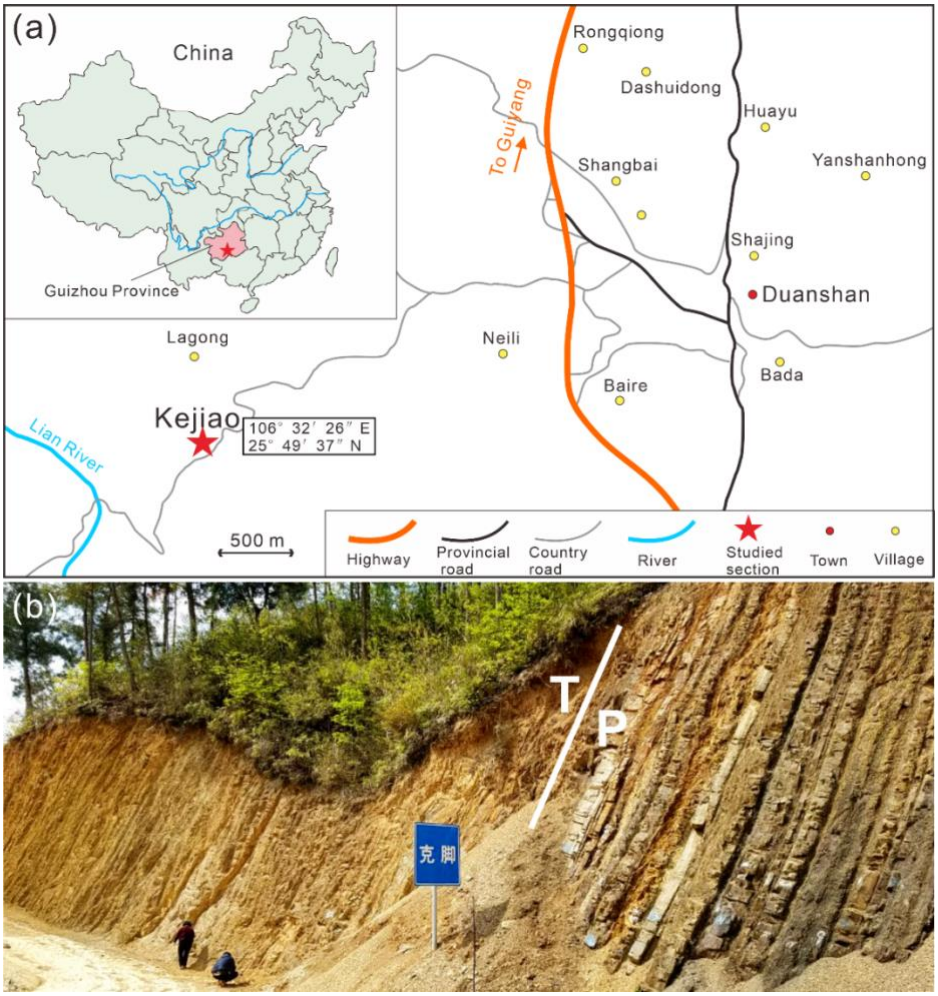

Supplementary Figure S1. (a) Location of the Kejiao section, Huishui County, Guizhou Province, South China. (b) Field photo showing the succession of the uppermost Permian Dalong Formation to the lowest Triassic Daye Formation in the Kejiao section. Note the Permian-Triassic boundary is marked as P/T in the field photo.

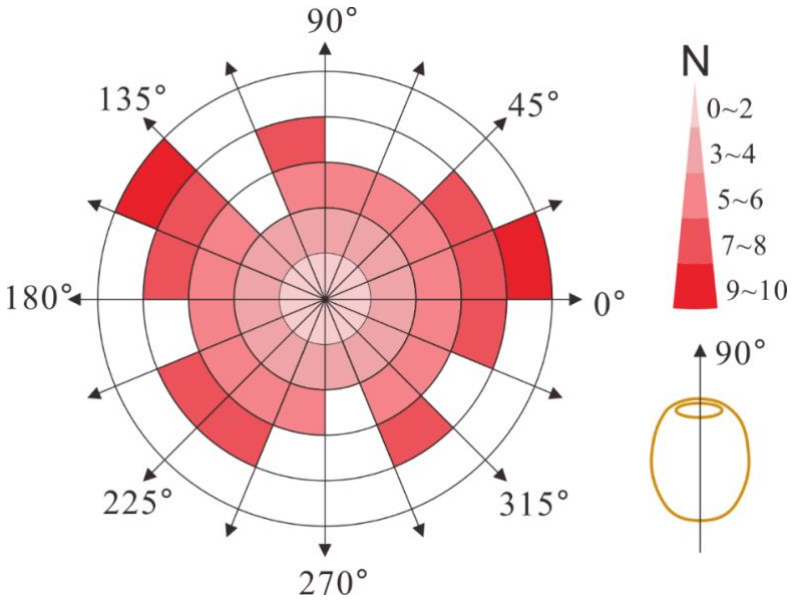

Supplementary Figure S2. Rose diagram shows orientation of sponge specimens distributed on the surface of one slab. N=104.

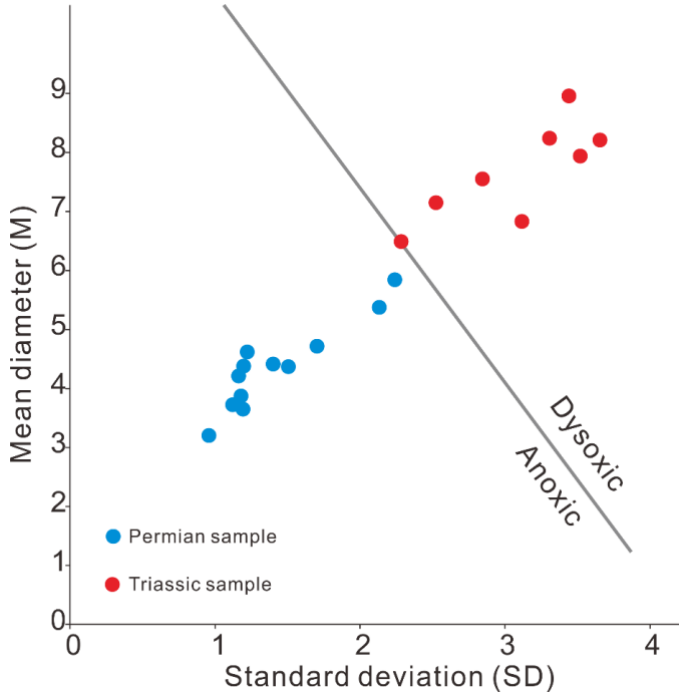

Supplementary Figure S3. M-SD plot of mean diameter versus standard deviation of pyrite framboid sizes for the Kejiao section (see pyrite framboid size distributions in Figure 2).

Relationship of the new fossil keratose sponge

The new taxon exhibits similarities of the fiber structure, especially the arrangement of thick primary and thinner secondary fibers, with modern taxa related to the Dictyoceratida (Minchin 1900) and specially with the Thorectidae erected by Bergquist 1978. The Thorectidae have various growth forms and show often vase- and mound shaped morphologies. In modern taxa the choanocyte chambers are characteristic and taxon specific which are not preserved in the fossil representatives. The spongin fibers of the Thorectidae often form an anastomosing skeleton (Fig. 4e, g). The central region of the primary thick fibers often shows a diffuse area often enriched with agglutinated material which is, however, not observed in the new sponge. Many primary fibers are often extremely thick and arranged with thinner, maybe secondary fibers, and form basket-like structures (Figures. 3-4). This spongin fiber arrangement is often seen in the new fossil sponge and resemble strongly to the fiber skeleton known from the Thorectidae. This was the main reason to classify the new taxon within the Thorectidae. The new fossil sponge is most similar to the modern genus *Smenospongia* first described by Wiedenmayer (1977) (Figure 4d-g). The irregular arrangements of the primary thick and thinner secondary fibers and prominent large oscular pores on top of the sponge baskets (Figures 3b-c, i-j, n, o; 4a-c, d) support this alignment.

Phylogenetic status of the aspiculate "keratose" demosponges.

The term "Keratosa" or "horny sponges" was introduced by Grant (1861), and was further elaborated by several workers (Bowerbank, 1866; Lendenfeld, 1889; Minchin, 1900). Biochemical and molecular phylogenetic data reveal that these sponges are probably the sister group of the spicular demosponges (Erpenbeck et al., 2020; Erpenbeck et al., 2012; Lavrov et al., 2008). Aspiculate demosponges are categorized as two clades: the "Keratosa" and Myxospongida. The former includes the orders Dictyoceratida and Dendroceratida, exhibiting organic skeletons made of spongin. Spongin is an enigmatic proteinaceous material that contains halogenated residues and

until recently had not been sequenced (Ehrlich, 2019). The latter embraces the orders Verongida, Halisarcida and Chondrosida, and forms chitinous fiber skeletons (Ehrlich et al., 2010; Ehrlich et al., 2013; Morrow and Cárdenas, 2015; Vacelet et al., 2019). Due to the widespread homoplasy in the skeletal morphology of these sponges (Erpenbeck et al., 2020; Vacelet et al., 2019) and the loss of biochemical information during taphonomic processes, it is hard to differentiate the two clades in fossil record.

Description of Holotype and Paratypes I, II and III

Holotype

BGEG KJ10301. The holotype (Figure 4a) is more or less spherical in outline, with 5 mm in width/horizontal diameter and 4.6 mm in vertical height. The main osculum has a diameter of nearly 2 mm. The margin of the oscular area is enhanced, typical for the main opening and shows an inner ring structure. The entire sponge skeleton looks like a basket. The organic skeleton fibers exhibit only one distinct front and rear network layer, caused by taphonomic compression of the sponge body. The organic fibers show clearly the main thick fibers of 200-250 μm in diameter. The thinner ones, developed from the thicker ones, are 50-150 μm in diameter. Generally, the fibers are crowded and anastomose. The spaces between the fibers show an average diameter of 400 μm–1mm. The fibers are composed of kerogenous-like black organic carbon without any allochthonous inclusions or spicules.

Paratype I

BGEG KJ10302. Paratype I (Figure 4b), 1.2 cm high and 0.8 cm wide, is larger and more elongated than the holotype. The network of the preserved fibers exhibits the same dimensions as the holotype. The fibers also anastomose and show thick and thinner ones. The spaces between the fibers show an average diameter of 0.5–1 mm. The central oscular area is not completely preserved and with a diameter of 5.3 mm wider than expected. The base of the sponge exhibits an enhancement of the fiber network and this

feature is interpreted as hold fast character. The fibers are also preserved in black organic carbon (kerogenous material).

Paratype II

BGEG KJ10303. Paratype II (Figure 4c), 1.3 cm wide and 1.53 cm high, is larger and more elongated than the holotype and paratype I. The network of the preserved fibers exhibits the same dimensions as the holotype and paratype I. The fibers also anastomose and show thick and thinner ones. The spaces between the fibers show an average diameter of 0.5–1 mm. However, the central part of the sponge is not very well preserved and the fiber skeleton is due to incomplete preservation. However, the central osculum is completely preserved and with a diameter of 4 mm. The margin of the oscular area is enhanced, typical for this opening. The base of the sponge also shows an enhancement of the fiber network and this feature is interpreted as a hold fast. The fibers are also preserved in black organic carbon (kerogenous material).

Paratype III

BGEG KJ103014. Paratype III (Figure 3i) has the appearance of a tower and has a height of 1 cm and a width of 5 mm. The oscular area is developed and the main osculum has diameter of 2 mm. The base of the sponge is irregular and fragmented. The spaces between the fibers vary from 300 µm to 1mm. Most of the fibers are between 100-250 µm thick. Thin fibres are rare. Part of the left fiber skeleton is damaged together with the basal areas. The sponge shows, on its right side a probable branch possibly representing an asexual bud. The base of the contact area with the mother sponge is well developed and does not exhibit anastomosing fibers. The branch is 6 high and 3 mm wide. The central osculum is not preserved and the top area is fragmented. The right lower part of the branch is not well preserved and the fiber structure is excised.

REFERENCES CITED

Bergquist, P. (1978). Sponges: University of California Press.

Bowerbank, J.S. (1866). A monograph of the British Spongiadae: The Ray Society, London.

Ehrlich, H. (2019). Marine biological materials of invertebrate origin (Vol. 13). Cham: Springer International Publishing.

Ehrlich, H., Ilan, M., Maldonado, M., Muricy, G., Bavestrello, G., Kljajic, Z., Carballo, J., Schiaparelli, S., Ereskovsky, A., & Schupp, P. (2010). Three-dimensional chitin-based scaffolds from Verongida sponges (Demospongiae: Porifera). Part I. Isolation and identification of chitin. International Journal of Biological Macromolecules, 47(2), 132-140. https://doi.org/10.1016/j.ijbiomac.2010.05.007

Ehrlich, H., Rigby, J. K., Botting, J., Tsurkan, M., Werner, C., Schwille, P., Petrášek, Z., Pisera, A., Simon, P., & Sivkov, V. (2013). Discovery of 505-million-year old chitin in the basal demosponge Vauxia gracilenta. Scientific reports, 3(1), 3497. https://doi.org/10.1038/srep03497

Erpenbeck, D., Galitz, A., Ekins, M., Cook, S. D. C., van Soest, R. W., Hooper, J. N., & Wörheide, G. (2020). Soft sponges with tricky tree: On the phylogeny of dictyoceratid sponges. Journal of Zoological Systematics and Evolutionary Research, 58(1), 27-40. https://doi.org/10.1111/jzs.12351

Erpenbeck, D., Sutcliffe, P., Cook, S. D. C., Dietzel, A., Maldonado, M., van Soest, R. W., Hooper, J. N., & Wörheide, G. (2012). Horny sponges and their affairs: On the phylogenetic relationships of keratose sponges. Molecular Phylogenetics and Evolution, 63(3), 809-816. https://doi.org/10.1016/j.ympev.2012.02.024

Grant, R. E., 1861, Tabular view of the primary divisions of the Animal Kingdom, intended to serve as an outline of an elementary course of recent zoology (caino-zoology); or, the natural history of existing animals, Walton and Maberly.

Lavrov, D. V., Wang, X., & Kelly, M. (2008). Reconstructing ordinal relationships in the Demospongiae using mitochondrial genomic data. Molecular phylogenetics and evolution, 49(1), 111-124. https://doi.org/10.1016/j.ympev.2008.05.014.

Lendenfeld, R. (1889). A monograph of the horny sponges, Royal Society. Trübner & Co., London.

Luo, C., Zhao, F., & Zeng, H. (2020). The first report of a vauxiid sponge from the Cambrian Chengjiang Biota. Journal of Paleontology, 94(1), 28-33. https://doi.org/10.1017/jpa.2019.52.

Minchin, E. A., & Lankester, E. R. (1900). Chapter III. Sponges. A treatise on zoology. Part II. The Porifera and Coelenterata, 2, 1-178.

Morrow, C., & Cárdenas, P. (2015). Proposal for a revised classification of the Demospongiae (Porifera). Frontiers in Zoology, 12, 1-27. https://doi.org/10.1186/s12983-015-0099-8

Vacelet, J., Erpenbeck, D., Diaz, C., Ehrlich, H., & Fromont, J. (2019). New family and genus for *Dendrilla*-like sponges with characters of Verongiida. Part I redescription of Dendrilla lacunosa Hentschel 1912, diagnosis of the new family Ernstillidae and Ernstilla ng. Zoologischer Anzeiger, 280, 14-20. https://doi.org/10.1016/j.jcz.2019.03.001

Wiedenmayer, F. (1977). Shallow-water sponges of the western Bahamas: Experientia Supplementum, 1-287.